Detecting Thalamic Abnormalities in Autism Using Cylinder Conformal Mapping

Qing He[1], Ye Duan[1], Xiaotian Yin[2], Xianfeng Gu[2], Kevin Karsch[1], and Judith Miles[3]

[1] Department of Computer Science, University of Missouri-Columbia, Columbia, MO, 65211, USA
[2] State University of New York at Stony Brook Stony Brook, New York 11794, USA
[3] Thompson Center for Autism, University of Missouri-Columbia, Columbia, MO, 65211, USA
qhgb2@mizzou.edu, duanye@missouri.edu, {xyin,gu}@cs.sunysb.edu, krkq35@mizzou.edu, MilesJH@missouri.edu

Abstract. A number of studies have documented that autism has a neurobiological basis, but the anatomical extent of these neurobiological abnormalities is largely unknown. In this paper, we applied advanced computational techniques to extract 3D surface models of the thalamus and subsequently analyze highly localized shape variations in a homogeneous group of autism children. In particular, a new conformal parameterization for high genus surfaces is applied in our shape analysis work, which maps the surfaces onto a cylinder domain. Surface matching among different individual meshes is achieved by re-triangulating each mesh according to the template. Children with autism and their controls are compared, and statistical significant abnormalities in thalamus of autism are detected.

1 Introduction

Autism is a spectrum of complex neurodevelopmental disorders of childhood defined by the presence of social deficits, abnormalities in communication, the presence of stereotyped, repetitive behaviors, and a characteristic course. Despite the large number of structural imaging studies in autism, results are generally inconclusive, and sometimes even contradictory. One possible reason is that heterogeneity within the autism diagnosis obscures the genetic basis of the disorder. Recently, Miles et al. proposed a new definition of autism subgroups, which divided autism into essential autism and complex autism [1]. In this paper, we limit our study to the essential autism group, which will greatly reduce the heterogeneous factors that cause inconsistent results [2].

Thalamus is the relay center for nerve impulses in the brain. A few studies have reported reduced thalamic volume in patients with autism [3, 4]. Moreover, [5, 6] have found abnormal relation between total brain volume and thalamic volume in autistic patients, in which the size of the thalamus did not increase as the brain size increased. Most of the previous works however only focused on volume analysis.

G. Bebis et al. (Eds.): ISVC 2008, Part II, LNCS 5359, pp. 743–751, 2008.

In this paper, we apply advanced computational techniques to extract 3D surface models of the thalamus and subsequently analyze highly localized shape variations. A semiautomatic segmentation method [7] is used to extract the 2D shapes of the thalamus instead of manual tracing. Contour stitching is performed in section 3 to produce a 3D surface, with two openings (i.e. boundary curves) at the ends. For surface matching, we apply a new conformal parameterization for high genus surfaces. This is followed by a statistical shape analysis that generates a significance map of the local morphologies.

Conformal parameterization has been explored intensively as a potential approach to the matching and analysis of brain data. It maps the brain surface into regular and simpler domain and carries out the analysis on the parameter domain. [8] used spherical conformal map to match cortical surfaces, where they parameterize the genus zero closed surfaces by spheres. Based on the shape characteristics of the two structures, we design a conformal method, called *cylinder map*, to parameterize the target surfaces with open cylinders and then match the points among them (Fig. 2).

2 2D Segmentation

We use the method in [7] to segment the thalamus from axial MR slices. This method has been applied to both 2D and 3D segmentation of the thalamus. However, there is no validation of the results of 3D segmentation in [7], and it is difficult to visually judge the accuracy of the 3D model. Therefore, instead of extracting the 3D thalamus model directly from the volume data, we start with slice-by-slice 2D segmentation and stack the 2D curves to make a 3D model. Because it is more straightforward to verify the accuracy of 2D results slice by slice, this method provides better results as opposed to direct 3D segmentation and validation.

This method is based on the concept of geometric surface flow. The general formulation is the following partial differential equation:

$$\partial \vec{s} / \partial t = F(t,k,...)\vec{n}(\vec{p},t), \vec{s}(\vec{p},0) = \vec{s}_0(\vec{p}) \tag{1}$$

where F is the speed function, t is the time variable, k is the surface curvature at the point $\vec{p}$, $\vec{s}_0(\vec{p})$ is the initial surface, and $\vec{n}$ is the surface normal vector. The speed function in [7] is defined as:

$$F = a_1(H_{current} - H_{average}) - a_2(\Delta(G_\sigma * I) + a_3 /(1+|\nabla B|^2) \tag{2}$$

where a_1, a_2, a_3 are coefficients for the three terms. The first term is the regular term to maintain the smoothness of the model. $H_{current}$ is the mean curvature at current surface point and $H_{average}$ is the average mean curvature of the whole model. The second term is the Laplacian (Δ)-Gaussian (G_σ) operation of the image I, which captures the edge information. The third term is the region information where ∇B is the gradient of a binary image created by the interior probability estimation of the current model. The details of the binary image B can be found in [7]. By integrating

edge and region information, this method can significantly alleviate the problem of the low contrast and discontinuous edges in MR images of the thalamus.

The algorithm starts with a user initialized seed contour inside the region of interest, and evolve the model according to (1) and (2). In [7], a pixel is selected by the user and a circular contour centered at the pixel is created to serve as the seed. In our implementation, we also allow the user to click several points to form an arbitrary closed contour as the seed (Fig. 1(a)). Fig. 1(b) shows the result of the segmentation.

We perform a quantitative evaluation of our method. We denote the correct segmentation result as C_{true}, our segmentation result as C_{seg}, and $|\bullet|$ as the area enclosed within the result. The measurements in [9,10,11] are used to compare our segmentation results with the ground truth.

1) True positive fraction (TPF):

$$TPF = |C_{seg} \cap C_{true}| / |C_{true}| \tag{3}$$

2) Dice similarity:

$$Dice = 2 \times |C_{seg} \cap C_{true}| / (|C_{true}| + |C_{seg}|) \tag{4}$$

3) Overlap coefficient:

$$overlap = |C_{seg} \cap C_{true}| / |C_{true} \cup C_{seg}| \tag{5}$$

The last two measurements range from 0 to 1 with one indicating a perfect agreement between C_{true} and C_{seg}. The overlap measurement is a stronger test than Dice similarity for segmentation accuracy [9].

We use the results of manual segmentation by a trained expert as the ground truth (C_{true}). The time for an experienced expert to segment the thalamus on one slice is about 10 minutes. The experiment is performed on MR images of 10 subjects, and the mean and standard deviation of each measurement across subjects are listed in Table 1. The table shows high means and low standard deviations in the three measurements, indicating high accuracy of our method.

Table 1. Quantitative validation results

	TPF	Dice	Overlap
Mean	0.85	0.83	0.78
Std	0.06	0.05	0.08


(a)

(b)

Fig. 1. (a) An arbitrary contour as the initial seed (b) The final segmentation result

3 3D Model Reconstruction

Contour stitching is performed to reconstruct the 3D model from 2D contours. For a set of thalamus contours to be connected, we do a uniform sampling on each contour to make them have the same number of points. In order to keep the accuracy of the contour, we first do a global subdivision [12] on each contour to make the points over dense. Suppose the average number of points across the contours after subdivision is n, and the smallest number of points among the contours is m. in order to balance the sample accuracy and model complexity, we uniformly sample n^* points on each contour, where $n^*=min(m, n/2)$. Now that every contour has the same number of points, we try every possible alignment of every two adjacent contours. For each alignment, we calculate the distance from each point on one contour to its corresponding point on the other contour. The best alignment is the one that minimize the sum of squared distances of all points.

By connecting the matched point pairs between adjacent contours, the 3D mesh is created with two openings at each end. A tangential Laplacian smoothing [13] is performed to maintain a good node distribution of the model. The reconstructed thalamus model is shown in Fig. 2.

4 Surface Matching

To build the one-to-one correspondence between two 3D surfaces, we parameterize both surfaces using an open cylinder. We first compute a conformal map from each given target mesh to a cylinder domain, then we align the two cylinders to find the point correspondence. Finally, we map the cylinder back onto the original surface to obtain the matching between two surfaces. Fig. 2 illustrates the process to match two thalamus surface meshes.

To map a target surface mesh T onto the cylinder domain T', we need a special holomorphic one-form $\eta + {}^*\eta\sqrt{-1}$, such that $\int_T \eta$ is constant along each boundary

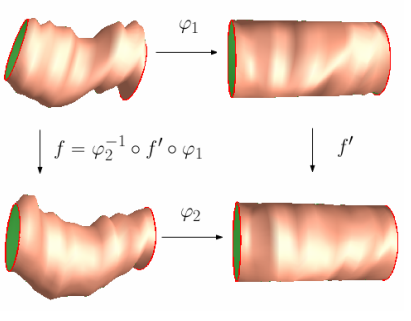

Fig. 2. Matching two thalamus surfaces (the left column) utilizing the cylinder domain (the right column)

curve while $\int_T {}^{*}\eta$ has a period of 2π around the boundary curves. This holomorphic one-form can be computed utilizing the techniques introduced in [14]. With the holomorphic one-form computed, the whole target surface is mapped to an open cylinder (see Fig. 4) with X axis as the axis, and the two boundary curves are mapped to two unit circles on the plane *x=0* and *x=h* respectively, where *h* is the length of the cylinder. Different target surfaces may have different *h* values in the cylinder domain, although the radius of the cylinder is always normalized to be 1.

After two surface meshes T_1 and T_2 are mapped to open cylinders T'_1 and T'_2, we can easily build a map *f'* between them. Firstly, a feature vertex (see the black point in Fig. 4) is marked on each cylinder so that they are matched to each other. Then, we rescale T'_2 along its axis so that the boundary curves are aligned with their counterparts in T'_1. Finally, T'_2 is rotated around its axis so that its marker vertex is aligned with that of T'_1. The rescaling is affine and the rotation is iso-metric, both of which are harmonic; their composition *f'* is therefore also harmonic.

Once a matching is computed on the parameter domain, we can pull it back onto the original surfaces to obtain the matching:

$$f = \varphi_2^{-1} \circ f' \circ \varphi_1 \tag{6}$$

Under this matching, each vertex $v \in T_1$ is mapped to an image point *f(v)* on T_2. Without loss of generality, each image point is represented as a pair <*face, bary*>, where *face* is the triangle containing the image point, and *bary* is a vector consisting of the corresponding barycentric coordinates of the image point. From this representation, the matching can be encoded in an alternative way by resampling T_2 with those image points and retriangulated using the connectivity of T_1. In other words, the triangulation of T_1 can be transferred onto T_2 while the geometry of T_2 can be preserved if the sampling is dense enough. In this way, for a group of meshes to be compared, we are allowed to unify the triangulation of each of them, which will simplify the latter analysis tasks.

5 Shape Analysis

Before the shape analysis, rigid-body Procrustes Analysis [15] is performed on each 3D mesh across subjects. The details algorithm can be found in [15]. In the local shape analysis, difference between groups at every surface location is tested. The difference in the size of the hippocampus has been eliminated in the spatial alignment, so the shape analysis only reveals pure shape difference between patients and controls. This can be done in two main fashions [16]. One way is to analyze the local difference to a template, which is usually the mean of the two groups. Student t-test can be used to test the local significance and [2] used this method. The main disadvantage of this method is the need to select a template, which introduces an additional

bias. The other method is to directly analyze the spatial location of each point, and we apply this method in our study. No template is needed in this approach and multivariate statistics of the (x,y,z) location is used. Hotelling T^2 two-sample metric is used to measure how two groups are locally different from each other. We use a modified T^2 metric instead of the standard one, because it is less sensitive to group differences of the covariance matrixes and the sample size [16]. This metric is defined as

$$T^2 = (\mu_1 - \mu_2)'((1/n_1)\sum_1 + (1/n_2)\sum_2))^{-1}(\mu_1 - \mu_2) \quad (7)$$

where $\sum_1$ and $\sum_2$ are the covariance matrixes of the two groups, and n_1 ,n_2 are the sample sizes. Since comparisons are made at thousands of hippocampal surface points, a permutation test is therefore used to confirm the significance of the overall differences in the statistical mapping result, adjusting for multiple comparisons. Suppose we have two groups whose sample sizes are n_1 and n_2, the permutation scheme can be stated as follows.

1. Calculate the test statistic (in our case, T^2) between the two groups, denoted as S_0.
2. The observations of the two groups are pooled. From the pooled values, n_1 observations are sampled without replacement to form group 1, and n_2 observations are sampled to form group 2. The test statistic between the two new groups is calculated.
3. Repeat the sampling process (permutation) in step 2 for M times. The test statistic in jth permutation is denoted as S_j.
4. The proportion of S_j's which are greater than S_0 is the p-value.

M is a large number and is set to 1000 in our experiment. The resulting p-values generate a significance map that locates significant shape differences between the two groups. Both raw and corrected p values are shown in the experiment.

6 Experimental Results

Ten children with autism and ten healthy children recruited from the NIH Human Brain Project participated in this study. The mean and standard deviation of the age of the subjects were 5.5 and 2.1. Axial, coronal and sagittal T1-weighted images were acquired using the Siemens Symphony 1.5 T scanner with the following parameters: TR = 35ms, NEX = 1, flip-angle = 30 degrees, thickness = 1.5mm, field of view = 22cm, matrix =512x512. Each brain volume was interpolated to 0.9-mm isotropic voxels.

6.1 Group Mean Difference Visualization

Fig. 3 gives a descriptive visualization of the group mean difference. The overlaid average structures of the left and right thalami are shown in Fig. 3(a). Fig. 3(b) shows the signed distance maps between the overlaid average structures on the overall average shape, with the same views as in Fig. 3(a). A positive distance (red) means the patients' structure is inside the controls' and a negative distance (blue) means the reverse case.

As shown in Fig. 3, the average thalamic shape of the patients is inside that of the controls in a larger portion (from the body to the posterior), and outside that of the controls in a smaller portion (most part of the anterior). This intuitive visualization coincides with the results of volumetric analysis in previous work, which reported reduced thalamic size [3-6] in autism.

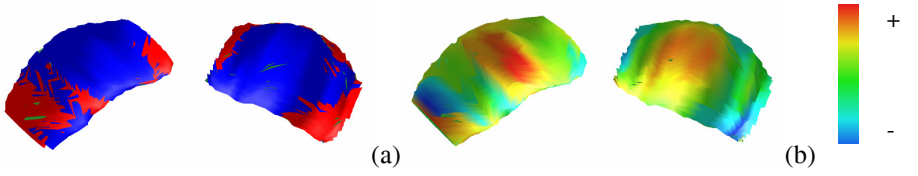

Fig. 3. (a) Two average structures (blue: controls, red: patients) (b) Distance map between the two averages (negative distances indicate the patients structure is outside the controls)

6.2 Statistical Testing Results

The significance maps after permutation tests are shown as color coded p-values in Fig. 4. Smaller p-values indicate larger statistical significance. A two-tailed alpha level of 0.05 is chosen as the significance threshold. More detailed local shape difference can be visualized in Fig. 4. Significant difference exists in the posterior body of both left and right thalami.

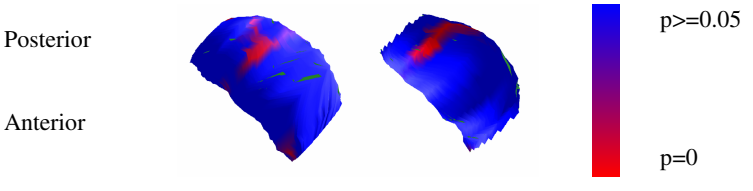

Fig. 4. Significance map with color coded p-value

7 Conclusion

We have applied advanced computational techniques to extract 3D surface models of the thalamus and subsequently analyze highly localized shape variations in a homogeneous group of autism children. In particular, a new conformal parameterization for high genus surfaces is applied in our shape analysis work, which maps the surfaces onto a cylinder domain. Surface matching among different individual meshes is achieved by re-triangulating each mesh according to the template. Children with autism and their controls are compared, and significant difference in the posterior body of both left and right thalami is found between autistic children and controls. Most previous studies on the thalamus only focus on volume changes, our work, however, has revealed local shape variations at precise surface locations.

The results of this paper need to be interpreted with caution because of the small sample size. Future work involves experiment on a larger sample and the comparison

of more features of the thalamus between patients and controls, such as the asymmetry patterns.

Acknowledgments. This work is supported in part by a NIH pre-doctoral training grant for Clinical Biodetectives, Thompson Center Research Scholar fund, Department of Defense Autism Concept Award, NARSAD Foundation Young Investigator Award.

References

1. Miles, J.H., Takahashi, T.N., Bagby, S., Sahota, P.K., Vaslow, D.F., Wang, C.H., Hillman, R.E., Farmer, J.E.: Essential versus complex autism: definition of fundamental prognostic subtypes. Am. J. Med. Genet. A(135), 171–180 (2005)
2. He, Q., Duan, Y., Miles, J.H., Takahashi, T.N.: Statistical Shape Analysis of the Corpus Callosum in Subtypes of Autism. In: IEEE 7th International Symposium on Bioinformatics & Bioengineering, Boston, Massachusetts, USA (2007)
3. Tsatsanis, K., Rourke, B., Klin, A., Volkmar, F., Cicchetti, D., Schultz, R.: Reduced thalamic volume in high-functioning individuals with autism. Biological Psychiatry 53(2), 121–129 (2003)
4. Waiter, G.D., Williams, J.H., Murray, A.D., Gilchrist, A., Perrett, D.I., Whiten, A.: A voxel-based investigation of brain structure in male adolescents with autistic spectrum disorder. Neuroimage 22(2), 619–625 (2004)
5. Hardan, A., Girgis, R., Adams, J., Gilbert, A., Keshavan, M., Minshew, N.: Abnormal brain size effect on the thalamus in autism. Psychiatry Research: Neuroimaging 147(2-3), 145–151 (2000)
6. Hardan, A., Girgis, R., Adams, J., Gilbert, A., Melhem, N.M., Keshavan, M., Minshew, N.: Brief Report: Abnormal Association Between the Thalamus and Brain Size in Asperger's Disorder. J. Autism. Dev. Disord. (2007)
7. Heckenberg, G., Xi, Y., Duan, Y., Hua, J.: Brain Structure Segmentation from MRI by Geometric Surface Flow. International Journal of Biomedical Imaging, 6 (2006)
8. Gu, X., Wang, Y., Chan, T., Thompson, P.M., Yau, S.: Genus Zero Surface Conformal Mapping and Its Application to Brain Surface Mapping. IEEE Transactions on Medical Imaging 23(8) (2004)
9. Bueno, G., Musse, O., Heitz, F., Armspach, J.P.: Three-dimensional segmentation of anatomical structures in MR images on large data bases. Magnetic Resonance Imaging 19(1), 73–88 (2001)
10. Chen, T.,, Metaxas, D.: A hybrid framework for 3D medical image segmentation. Medical Image Analysis 9(6), 547–565 (2005)
11. Yushkevich, P.A., Piven, J., Hazlett, H.C., Smith, R.G., Ho, S.: User-guided 3D active contour segmentation of anatomical structures: significantly improved efficiency and reliability. NeuroImage 31(3), 1116–1128 (2006)
12. Belyaev, A.G., Anoshkina, E.V., Yoshizawa, S., Yano, M.: Polygonal curve evolutions for planar shape modeling and analysis. International Journal of Shape Modeling 5(2), 195–217 (1999)
13. Duan, Y., Hua, J., Qin, H.: Interactive shape modeling using lagrangian surface flow. The Visual Computer 21(5), 279–288 (2005)

14. Gu, X., Yau, S.: Global conformal surface parameterization. In: Proc. ACM Symp. Geometry Processing, pp. 127–137 (2003)
15. Ross A.: Procrustes analysis, Technical Report, Department of Computer Science and Engineering, University of South Carolina, SC 29208, http://www.cse.sc.edu/~songwang/CourseProj/proj2004/ross/ross.pdf
16. Styner, M., Oguz, L., Xu, S., Brechbuehler, C., Pantazis, D., Levitt, J.J., Shenton, M.E., Gerig, G.: Framework for the Statistical Shape Analysis of Brain Structures using SPHARM-PDM. In: ISC/NA-MIC Workshop on Open Science at MICCAI (2006)